Acta Crystallographica Section D
Biological Crystallography
ISSN 0907-4449

Structure of internalin C from *Listeria monocytogenes*

Amy Ooi,‡ Syeed Hussain,§ Arefeh Seyedarabi and Richard W. Pickersgill*

School of Biological and Chemical Sciences, Queen Mary, University of London, Mile End Road, London E1 4NS, England

‡ Current address: School of Biological Sciences, Nanyang Technological University, 60 Nanyang Drive, Singapore 637551.
§ Current address: Department of Biochemistry and Molecular Biology, University College London, Gower Street, London WC1E 6BT, England.

Correspondence e-mail: r.w.pickersgill@qmul.ac.uk

Received 3 May 2006
Accepted 10 July 2006

PDB Reference: internalin C, 1xeu, r1zeusf.

The crystal structure of internalin C (InlC) from *Listeria monocytogenes* has been determined at 2.0 Å resolution. Several observations implicate InlC in infection: *inlC* has the same transcriptional activator as other virulence genes, it is only present in pathogenic *Listeria* strains and an *inlC* deletion mutant is significantly less virulent. While the extended concave receptor-binding surfaces of the leucine-rich repeat (LRR) domains of internalins A and B have aromatic clusters involved in receptor binding, the corresponding surface of InlC is smaller, flatter and more hydrophilic, suggesting that InlC may be involved in weak or transient associations with receptors; this may help explain why no receptor has yet been discovered for InlC. In contrast, the Ig-like domain, to which the LRR domain is fused, has surface aromatics that may be of functional importance, possibly being involved in binding to the surface of the bacteria or in receptor binding.

1. Introduction

Listeria monocytogenes is a Gram-positive food-borne bacterium capable of causing severe infections in immunocompromized individuals, giving rise to septicaemia, meningitis or meningoencephalitis. The bacterium induces its own uptake into cells with low phagocytic activity, using the 'zipper' mechanism in which direct interaction between the bacterial surface proteins and the plasma membrane-bound host receptor proteins leads to invasion of the host cell. Two proteins that have been demonstrated to facilitate bacterial entry into human cells are internalins A and B (InlA and InlB). InlA, which is covalently linked to the surface of the bacterium as a result of its C-terminal LP*X*TG motif, typically promotes the infection of human enterocyte-like cell lines through interaction with the cellular receptor E-cadherin (Mengaud *et al.*, 1996). InlB, which is non-covalently bound to the surface of the bacterium *via* an association of its GW domains with bacterial cell-wall lipoteichoic acids, has a wider host-cell spectrum (Braun *et al.*, 1998; Parida *et al.*, 1998) and promotes phagocytosis by activation of phosphatidylinositol-3-kinase (Ireton *et al.*, 1996) in response to binding gC1q-R and a Met receptor tyrosine kinase (Braun & Cossart, 2000; Shen *et al.*, 2000).

Most virulence genes in *L. monocytogenes* are in a cluster controlled by the transcriptional activator PrfA (Leimeister-Wachter *et al.*, 1990; Mengaud *et al.*, 1991). The *inlAB* operon is also regulated by additional promoters. The *inlC* gene was discovered in a *prfA*-enriched/PrfA-regulated gene-cluster knockout of *L. monocytogenes* (Engelbrecht *et al.*, 1996), the result of a search for additional PrfA-regulated genes and their protein products. These authors showed that the *inlC* gene is transcribed into a monocistronic mRNA from a single

promotor with typical consensus sequence for PrfA-binding and encodes a small secreted protein of 297 residues. The *inlC* deletion mutant showed significantly reduced virulence in an intravenous mouse model, suggesting that InlC contributes to infection. The authors argued that InlC may be important in the later stages of infection. Subsequently, it emerged that there are two promoters for *inlC*, a PrfA-independent promoter in addition to the previously discovered PrfA-dependent promoter (Luo *et al.*, 2004); these authors suggest the PrfA-independent transcription of *inlC* may allow invasion of the bacteria into neighbouring host cells, whereas PrfA-dependent transcription has been shown to facilitate the action of InlA in cell invasion (Bergmann *et al.*, 2002). Engelbrecht *et al.* (1998) suggest that the *inlC* gene has been transferred between invasive *Listeria* species by horizontal gene transfer. Several observations support the importance of *inlC* in infection: (i) *inlC* is PrfA-regulated and InlC promotes InlA-mediated cell invasion (Engelbrecht *et al.*, 1998; Bergmann *et al.*, 2002), (ii) the *inlC* gene is present in pathogenic but not in non-pathogenic *Listeria* (Engelbrecht *et al.*, 1998) and (iii) the *inlC* deletion mutant has reduced virulence in a mouse model (Engelbrecht *et al.*, 1998). In this paper, we report the crystal structure of InlC and compare its surface characteristics with those of InlA and InlB. The surface of the Ig-like domain of internalin C is significantly richer in external hydrophobic residues compared with internalins A and B and these residues may be important for the function of InlC.

2. Materials and methods

2.1. Construction of the expression plasmid pET14b::*inlC*

The full coding sequence of internalin C (Engelbrecht *et al.*, 1996) was amplified from a pQE-30::*inlC* expression vector using the following two oligonucleotide primers: forward (5′-CTT**CATATG**GAGAGTATTCAACGACCAACG-3′) and reverse (5′-CTT**GGATCC**TAATTCTTGATAGGTTGTG-3′). The forward and reverse oligonucleotides incorporated *Nde*I and *Bam*HI restriction sites at their 5′-ends, respectively (the restriction sites are indicated in bold). A Perkin–Elmer 9600 thermal cycler was used for the PCR using a total reaction volume of 50 µl with 25 cycles of amplification using 2.5 U of HotStar *Taq* polymerase (Qiagen). The PCR product (789 bp) was gel purified using a spin column (Qiagen) and ligated into the pGEM-T Easy (Promega) vector before subcloning into pET-14b. Use of the pGEM-T Easy vector increased ligation efficiency and enabled blue/white selection of transformants in *Escherichia coli* JM109 cells. Verification of the presence of the *inlC* gene sequence was accomplished using *Eco*RI restriction digest and the gene was subsequently sequenced. Construction of the His-tagged fusion protein expression plasmid was achieved by subcloning the *inlC Nde*I/*Bam*HI fragment from the pGEM-T Easy construct into the analogous sites in pET-14b (Novagen), resulting in the plasmid construct pET-14b::*inlC*. This construct was transformed into the expression host, *E. coli* BL21 (DE3) pLysS (Novagen). An overnight culture was used to inoculate a 1 l shake flask of LB and overexpression of InlC was promoted after 2 h of preculture ($A_{600} \simeq 0.5$) by the addition of isopropyl thio-β-D-galactoside (IPTG) to a final concentration of 0.04 m*M*. 4 h after induction with IPTG, cells were harvested by centrifugation and the resulting cell pellet was solubilized in 20 ml 25 m*M* Tris–HCl pH 8.0 containing 1 *M* NaCl. Total soluble cell protein was isolated by sonication and clarification of the resulting solution from insoluble particulates by centrifugation.

Table 1
Data-collection and refinement statistics.

Values in parentheses are for reflections in the highest resolution shell.

	Crystal 1	Crystal 2
Data reduction		
Resolution range (Å)	30.0–2.5	30.0–2.0
Unique reflections	16272	24878
Completeness	94.2 (90.8)	87.7 (77.2)
Multiplicity	5.2	3.6
$R_{\rm merge}(I)$† (%)	4.5 (7.2)	9.1 (48.4)
Mean $I/\sigma(I)$	24.5 (10.6)	16.3 (2.2)
Mean B from Wilson plot (Å^2)	21.8	26.9
Molecular replacement		
Model I‡		
Correlation coefficient	0.223	—
R factor (%)	56.3	—
Model II‡		
Correlation coefficient	0.318	—
R factor (%)	53.4	—
Refinement		
R.m.s.d. bond lengths [σ] (Å)	0.023 [0.2]	0.014 [0.2]
R.m.s.d. bond angles [σ] (°)	2.139 [2.0]	1.645 [2.0]
R.m.s.d. torsion angles, period 1 [σ] (°)	5.1 [3.0]	4.4 [3.0]
Chiral centre restraints [σ] (Å^3)	0.125 [0.2]	0.101 [0.2]
R factor§ (%)	21.1	20.0
$R_{\rm free}$§ (%)	25.8	24.3
No. of amino-acid residues	263	263
No. of waters	87	226
Ramachandran plot statistics (%)		
Most favoured	81.9	80.6
Allowed	17.7	19.0
Generously allowed	0.4	0.4
Disallowed	0.0	0.0

† $R_{\rm merge} = \sum_h \sum_i |I_i(h) - \langle I(h)\rangle| / \sum_h \sum_i I_i(h)$, where $I_i(h)$ is the ith measurement of reflection h and $\langle I(h)\rangle$ is the weighted mean of all measurements of h. ‡ Search models I and II were InlB and InlB truncated by the removal of one coil of the LRR domain, respectively. The molecular-replacement solution was similar for both models, but the correlation coefficient was substantially more convincing for model II. § $R = \sum_h |F_{\rm obs} - F_{\rm calc}| / \sum_h F_{\rm obs}$, where $F_{\rm obs}$ and $F_{\rm calc}$ are the observed and calculated structure-factor amplitudes, respectively. The R factor and $R_{\rm free}$ were calculated using the working (95% of the data) and test set (5% of the data), respectively.

2.2. Purification of internalin C

Purification of InlC to homogeneity was achieved *via* a two-step purification procedure. The soluble crude protein extract described above was applied onto a Chelating Sepharose Fast-Flow (Pharmacia) column (4 × 1 ml) which had been charged with Ni^{2+} ions and equilibrated with 25 m*M* Tris–HCl buffer pH 8.0 containing 1.0 *M* NaCl and 10 m*M* imidazole. Nonspecifically bound proteins were eluted using 25 m*M* Tris–HCl buffer pH 8.0 containing 0.1 *M* NaCl and 50 m*M* imidazole. Bound protein, mainly comprising of histidine-tagged InlC, was eluted using 25 m*M* Tris–HCl buffer pH 8.0 containing 0.1 *M* NaCl and 500 m*M* imidazole in 1 ml fractions and assessed for protein content spectrophotometrically at

280 nm. The His tag was cleaved using thrombin. A Superdex-75 size-exclusion column equilibrated with 25 m*M* Tris–HCl buffer pH 8.0 containing 25 m*M* NaCl was used for the final purification step. SDS–PAGE revealed a single band migrating at approximately 30 kDa. The protein was concentrated to 20 mg ml^{-1} for crystallization.

2.3. Crystallization, data collection and structure determination

Crystallization trials utilized two commercially available screens, Hampton Research Crystal Screens I and II, and used the hanging-drop vapour-equilibration method with 2 µl drops. These crystals could be grown fairly reliably using stock reagents and the crystals diffracted to 2.5 Å resolution at room temperature using synchrotron radiation when mounted in a glass capillary. The crystals could be cryocooled by fast transfer through a solution corresponding to reservoir supplemented with 25% glycerol and these crystals were used for data collection at 100 K. Diffraction data to 2.5 Å, comprising 300 images each corresponding to a 0.5° rotation of the crystal, were recorded using crystal 1 and PX9.6 at SRS Daresbury (λ = 0.87 Å) equipped with an ADSC image plate. The diffraction data were processed using *DENZO* and *SCALEPACK* (Otwinowski & Minor, 1997) and the *CCP*4 program suite was used for subsequent calculations (Collaborative Computational Project, Number 4, 1994). The structure was solved by molecular replacement using *MOLREP* (Vagin & Teplyakov, 1997) and the structure of internalin B (Schubert *et al.*, 2001) that had been solved by molecular replacement using the structure of the LRR domain (Marino *et al.*, 1999). The 2.5 Å model of InlC was built using iterative cycles of building into σ_A-weighted $2F_{obs} - F_{calc}$ maps using *O* (Jones *et al.*, 1991) and refinement using *REFMAC* (Murshudov *et al.*, 1997). The final model was refined against subsequently collected 2.0 Å data and had an *R* factor of 21.1% (R_{free} = 25.8%) and contains 263 residues (35–297) and 226 water molecules. Model stereochemistry was evaluated using the program *PROCHECK* (Laskowski *et al.*, 1993). A total of 80.6% of residues are in the core regions of the Ramachandran plot, with no residues in disallowed regions. The data-collection and refinement statistics are summarized in Table 1.

3. Results and discussion

3.1. Structure determination

Crystals grew as thin plates of maximum dimension 0.5 mm from the trial with reservoir containing 1.8 *M* magnesium sulfate, 0.1 *M* MES pH 6.5. The systematic absences were consistent with space group $P2_12_12$, which was confirmed by molecular-replacement results, with unit-cell parameters

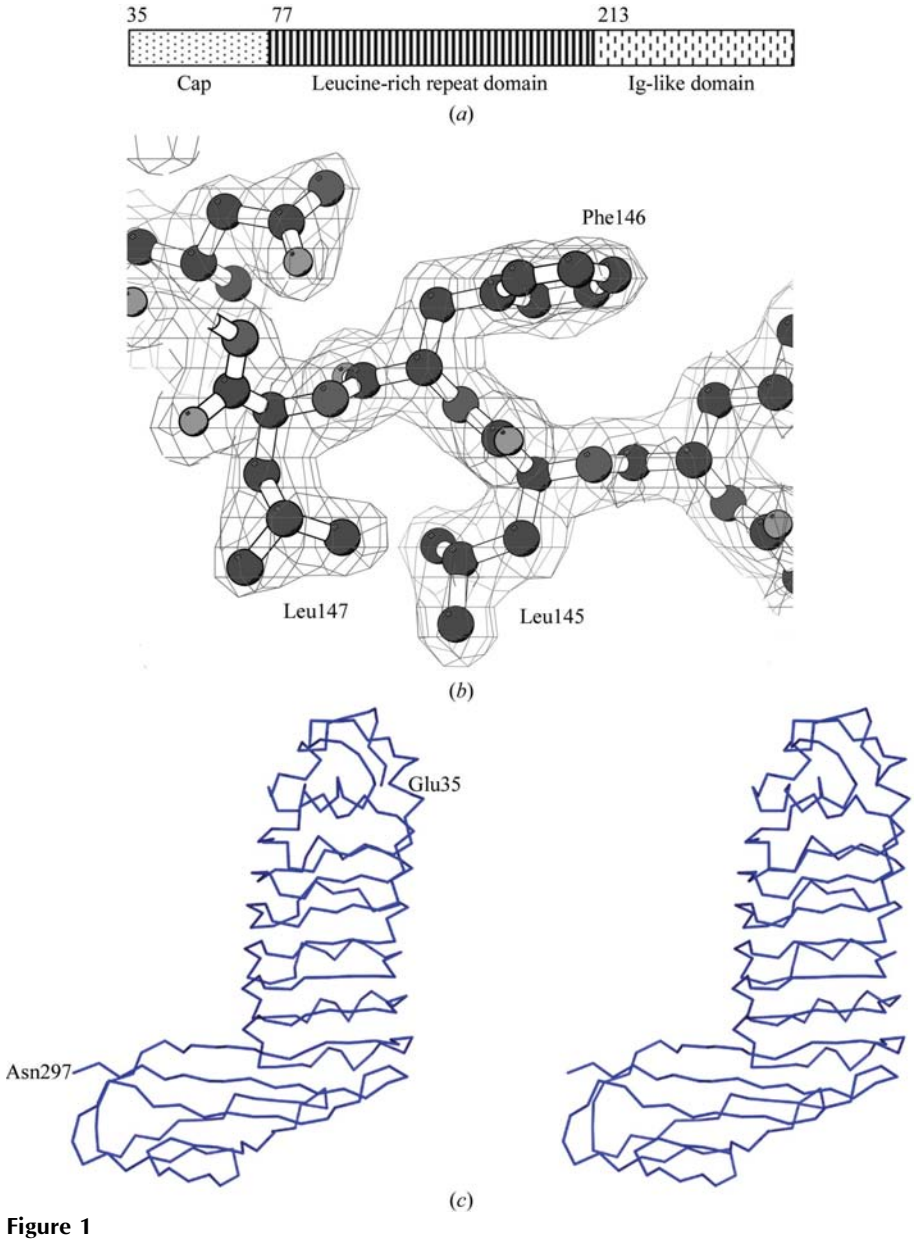

Figure 1
(*a*) Schematic drawing of the domain structure of internalin C. (*b*) Electron density around Phe146, one of only two exposed hydrophobic residues on the receptor-binding surface of internalin C; also shown are adjacent leucine residues that contribute to the hydrophobic core of the LRR domain. The 2.0 Å resolution σ_A-weighted $2F_{obs} - F_{calc}$ map was contoured at 1σ. (*c*) Stereo C^{α} trace of the internalin C structure. (*b*) was prepared using *BOBSCRIPT* (Esnouf, 1997) and (*c*) and Fig. 4(*b*) were prepared using *PyMOL* (DeLano, 2002).

a = 58.78, b = 179.51, c = 42.26 Å, with the asymmetric unit containing one InlC molecule and comprising approximately 65% solvent. Using the internalin domain of InlB (PDB code 1h6t), the closest structure in the PDB, with 34% sequence identity to InlC, as the search model in molecular replacement gave a correlation coefficient of only 0.223; however, if the third coil of the LRR domain was removed and a 'shortened' InlB molecule produced then the correlation improved significantly to 0.318 (Table 1). The electron-density maps were sufficiently clear and lacking in bias to allow cycles of rebuilding and refinement to give a final map in which all residues of InlC could be clearly seen. Subsequently, the structure was refined against the 2.0 Å data collected from a second crystal (over 30 crystals were screened to find two well diffracting ones) and the statistics for both refinements are presented in Table 1.

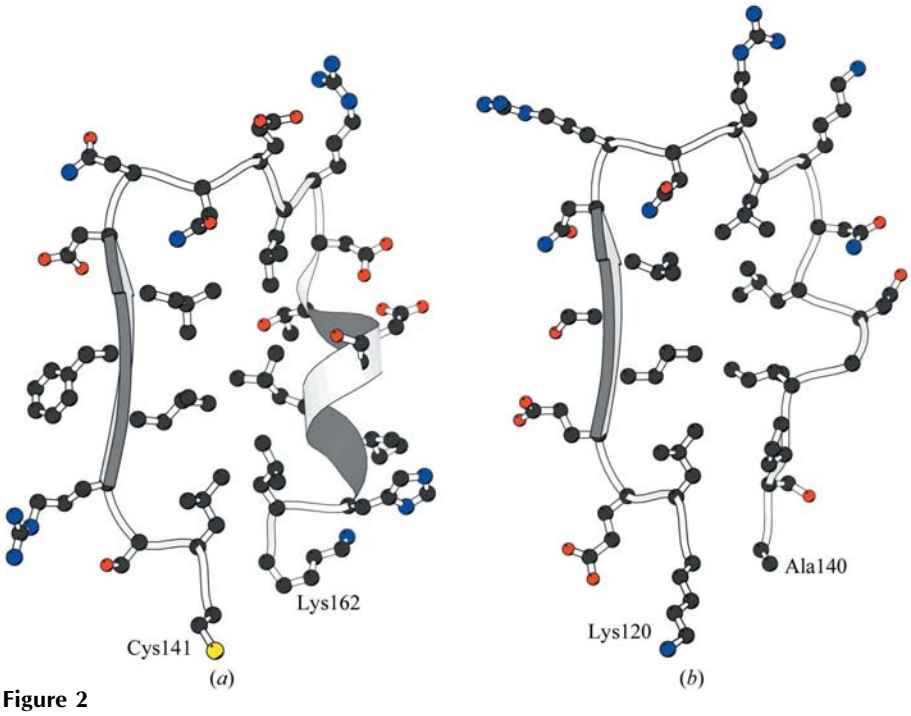

Figure 2
(*a*) Structure of a typical LRR coil of internalin C, comprising 22 residues. The LRR shown is coil four of six present in InlC and corresponds to residues 141–162. The hydrophobic core of the LRR domain is typically formed by leucine residues at positions 2, 5, 7, 12, 15, 18 and 21. There is an asparagine at position 10 in five out of the six turns; the first turn is a variant and the first β-strand of the Ig-like domain provides an equivalent glutamine. (*b*) Structure of the unique 21-residue coil three of InlC (residues 120–140). The 3_{10}-helix of the other coils (see *a*) is missing, replaced by a β1–4 turn (residues 15–18) and a proline at position 19.

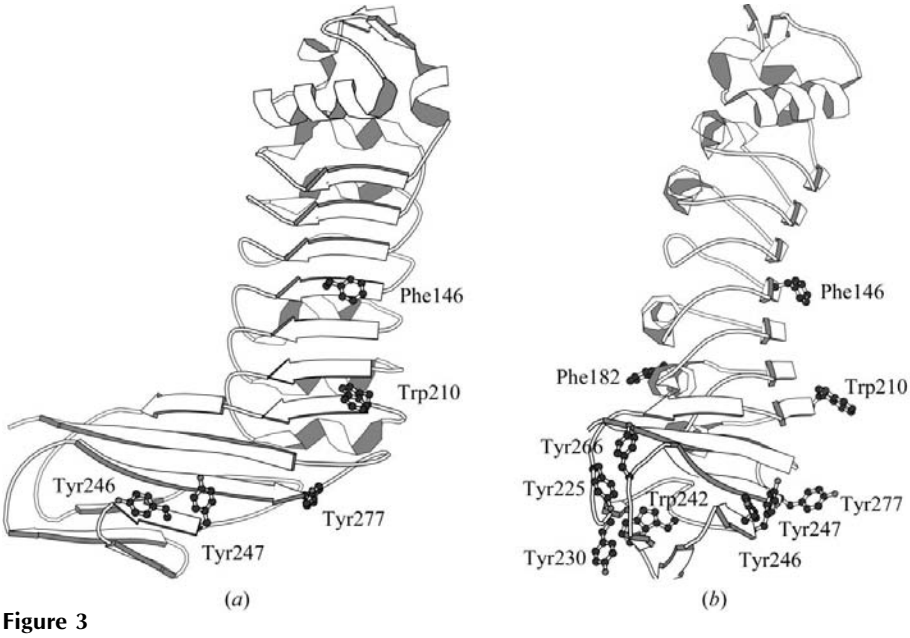

Figure 3
Schematic drawings of the structure of internalin C showing α-helices, 3_{10}-helices, β-strands and surface aromatic residues (*a*) looking down onto the parallel β-sheet with selected surface aromatics drawn in ball-and-stick representation (Phe146, Trp210, Tyr246, Tyr247 and Tyr277) and (*b*) perpendicular to the first view showing the slight curve of InlC and with Phe182, Tyr225, Tyr230, Trp242 and Tyr266 drawn in addition to the aromatics shown in (*b*). This figure and Fig. 4(*a*) were prepared using *MOLSCRIPT* (Kraulis, 1991).

3.2. Overall structure

InlC comprises an α-helical cap, a leucine-rich repeat (LRR) and immunoglobulin-like (Ig-like) domains (Fig. 1) as revealed for other members of the internalin family (Schubert *et al.*, 2001, 2002). The cap domain, residues 35–76, contains three α-helices and two very short β-strands. The LRR domain, residues 77–213, has right-handed superhelical architecture comprising six repeats, each with 22 residues per repeat except for coil three, which has 21 residues. A conserved pattern of internal aliphatic residues and an asparagine directed internally characterizes each repeat (Fig. 2). Each LRR tends to have leucine, isoleucine or valine at positions 5, 7, 12, 15, 18 and 21 of the coil, although some variation is possible. A typical coil comprises a five-residue β-strand and, less strictly, a five-residue 3_{10}-helix (Fig. 2*a*). In turn three the 3_{10}-helix is shortened and the aliphatic residue at position 21 is absent (Fig. 2*b*). The asparagine at position 10 appears to be important as it forms a buried asparagine ladder within the LRR domain. YopM, a LRR protein from *Yersinia pestis*, has 12 repeats of 20 residues and three of 22 residues (Evdokimov *et al.*, 2001). There is a single 21-residue repeat in InlA that confers functionally important flexibility to the molecule by disrupting the

Table 2
Intermolecular contacts in internalin C crystals.

Residue and atom in molecule *A*	Second molecule†	Residue and atom in contact	Separation (Å)
Tyr230 CD	*B*	Phe182 CZ	3.7
Tyr230 CE2	*B*	Met179 CE	3.7
Asp256 OD2	*B*	His160 ND1	2.6
Cys258 CB	*B*	Phe182 CE3	3.7
Trp242 CH2	*B*	Lys162 CE	3.9
Tyr246 CE1	*C*	Arg144 CD	3.9
Tyr247 CE2	*C*	Val188 CG1	3.7
Tyr247 OH	*C*	Asp190 OD2	2.7
Phe146 CZ	*C*	Tyr246 O	3.9
Ile166 CG1	*D*	Tyr246 CE1	3.7
Val188 CG1	*D*	Tyr247 CE2	3.7
Trp210 CZ2	*D*	Ser249 CB	3.4
Leu68 CD1	*E*	Pro42 CG	3.5
Pro42 CG	*E*	Leu68 CD1	3.5
Val265 CG2	*F*	Glu165 OE2	3.9

† The operators used to generate the symmetry-related molecules are $x + 1/2, -y + 1/2, 1 - z$ (molecule *B*), $x - 1/2, -y + 1/2, -z$ (molecule *C*), $x + 1/2, -y + 1/2, -z$ (molecule *D*), $1 - x, -y, z$ (molecule *E*) and $1 + x, y, z$ (molecule *F*).

Table 3
Structures similar to internalin C.

The similarity as detected by *DALI* (Holm & Sander, 1993) is given, but only structures with a *Z* score of more than 10 are listed. R.m.s.d. is the root-mean-square deviation of aligned C^{α} atoms. The proteins listed all contain a leucine-rich repeat domain which aligns with that of InlC. Full protein details are available from the *DALI* server or the PDB using the PDB codes given.

Protein name (PDB code)	*Z* score	R.m.s.d. (Å)	Residues aligned	Sequence identity (%)
Internalin B (1d0b)	26.3	1.9	202	34
Internalin A (1o6s)	17.8	2.8	176	26
Glycoprotein Ib α (1m0z)	15.7	2.7	163	25
Biglycan (2ft3)	15.2	2.6	160	19
LRIM (2a6f)	14.3	4.3	159	6
YopM (1jl5)	13.6	2.9	162	19
Rab transferase α subunit (1dce)	13.6	2.0	114	25
Toll-like receptor 3 (1ziw)	13.3	2.8	157	22
Slit protein (1w8)	13.2	2.7	147	18
U2 RNA hairpin IV (1a9n)	12.2	3.0	130	25
Skp2-fragment (1fqv)	11.4	4.4	171	18
GTPase-activating protein (1yrg)	11.0	3.9	170	18
Ribonuclease inhibitor (1a4y)	10.9	3.7	177	19

β-sheet locally (Schubert *et al.*, 2002). The deletion in InlC shortens the 3_{10}-helix and if it is of functional significance then it may be in flattening the putative receptor-binding surface. Residues 207–297 form an Ig-like domain, with *afgc* and *deb* β-sheets. In fact, because the domains are fused together, the last few residues of one domain are also the beginning of the next, as the residues form one contiguous structure.

3.3. Putative receptor-binding surface

The concave face of the β-sheet of the internalins has long been considered to be the binding surface by analogy with ribonuclease inhibitor protein (Kobe & Deisenhofer, 1995) and this has been demonstrated for InlA in its complex with E-cadherin (Schubert *et al.*, 2002). Surface-exposed aromatic residues dominate the direct interactions of the InlA LRR with E-cadherin and aromatic residues have also been shown to be important in the interaction of the LRR domain of InlB with the Met receptor (Machner *et al.*, 2003). The corresponding putative binding surface of InlC is flat compared with the concave surfaces of InlA and InlB, partially because InlC has the shortest LRR domain with only six repeats, compared with eight and 15 for InlB and InlA, respectively, but also because of the irregular nature of the 3_{10}-helices, including the truncated helix in repeat three. The surface of

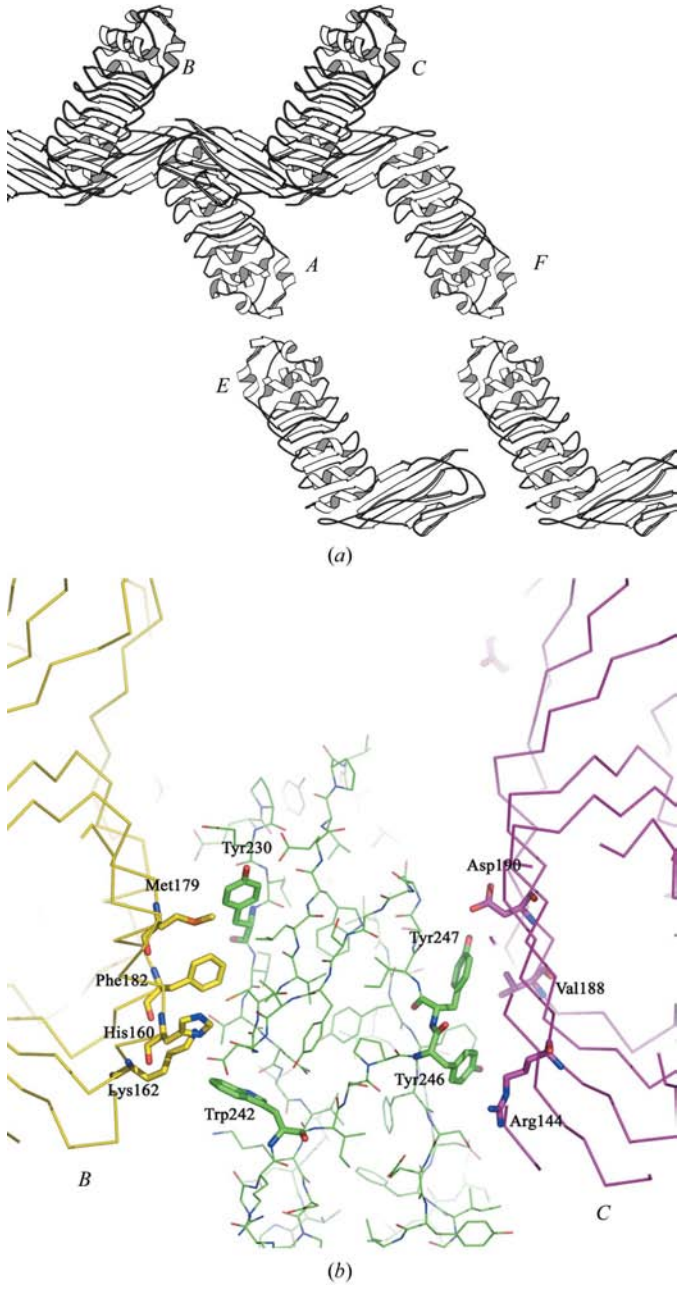

Figure 4
(*a*) The crystal packing of internalin C molecules viewed down the twofold axis, showing the open packing of the molecules in the crystal lattice when viewed in this direction. The figure shows that it is the Ig-like domain that is involved in the crystal contacts. The cap domain is involved in an association across the twofold involving Pro42 and Leu68, but there are few contacts involving the LRR domain. (*b*) A closer view of the aromatics involved in the packing of the Ig-like domains in the crystal.

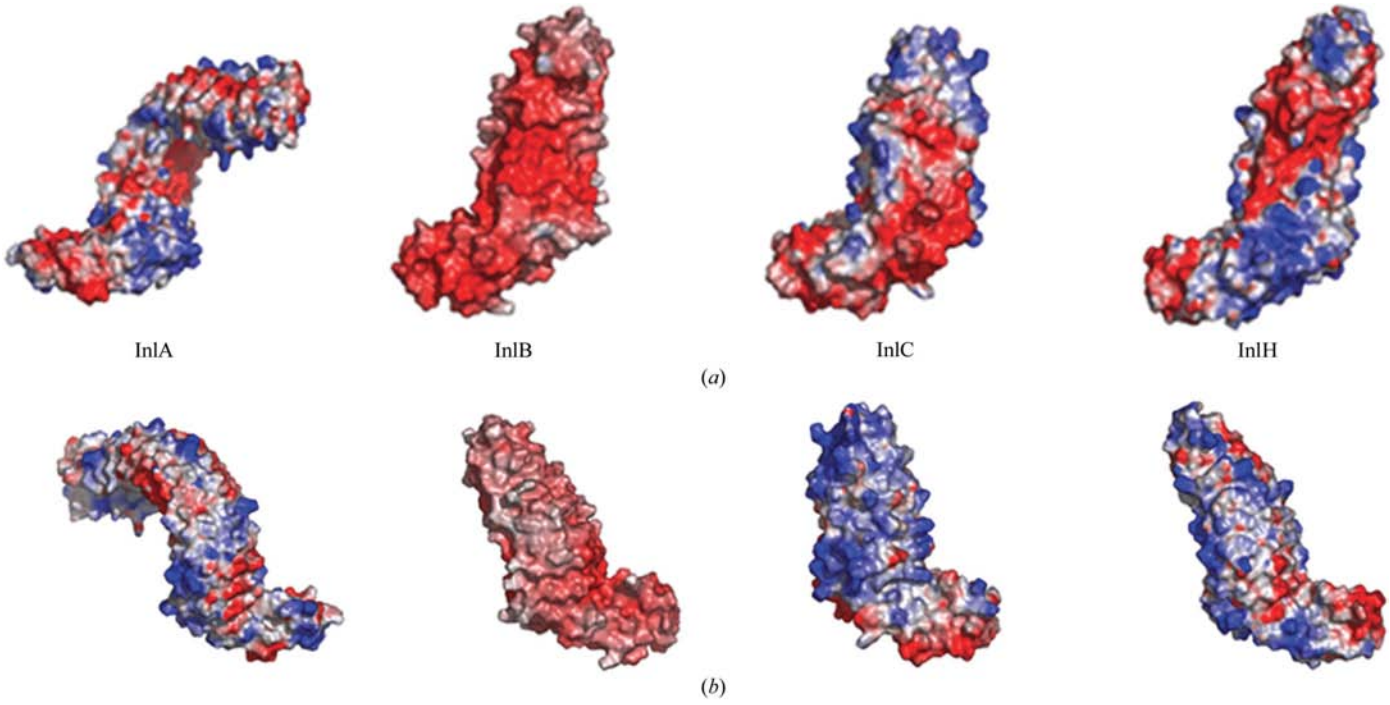

Figure 5
Surface-charge distribution of the solved internalin structures. Positive charge is in blue and negative in red. The proteins are not drawn to scale. (*a*) The concave surface-charge distribution of internalins A, B, C and H, showing the highly negatively charged concave binding pocket seen in all four members of the internalin family. This concave region has been shown to be the binding cleft for internalin A and its receptor E-cadheirin. (*b*) The convex side of the leucine-rich repeat domain, showing a more neutral and basic surface charge, except for InlB, which has a rather negative overall surface charge. The cap regions of InlA, C and H are comparatively positive, with scattered negative charges on the Ig-like domains.

the LRR domain is principally hydrophilic with only two exposed hydrophobic residues, Phe146 on the fourth β-strand of the LRR domain and Phe182 on the fifth 3_{10}-helix of the LRR domain (Fig. 3). There is no obvious similarity in the pattern of hydrophobic residues or charged residues when the proposed binding surface is compared with those of InlA or InlB. Aromatic contacts are also important in binding the GW domains of InlB to glycosaminoglycans and gC1q-R (Marino *et al.*, 2002).

3.4. Crystal packing

With few exceptions, the surface aromatic residues on the surface of InlC are either directly involved in crystal contacts or are very close to a crystal contact (Table 2; Fig. 4). The contacts therefore principally involve the Ig-like domain, with fewer contacts to the C-terminal part of the LRR domain and no contacts to the N-terminal part, mirroring the pattern of exposed aromatics (Fig. 3). The cap domain makes a contact with its twofold-related symmetry mate involving Pro42 and Leu68 (Fig. 4). Hydrogen bonds are involved in crystal contacts with molecules *B* and *C* (Table 2).

3.5. Functional implications

The most similar structures in the PDB are InlB and InlA, with other structures with LLR domains also being detected by *DALI* (Holm & Sander, 1993; Table 3). Comparison of the structure of InlC with InlA and InlB reveals no commonality in their surface features; there is no conserved pattern of hydrophobic residues and no common charge distribution (Fig. 5), in agreement with the observation that InlC binds to a different receptor to those bound by InlA and InlB. The N-terminal end of the molecule and especially the Ig-like domain is where the aromatic residues are concentrated and this region might self-associate as seen in the crystal or it might associate with other proteins. It is possible that the Ig-like domain associates loosely with the bacterial cell wall. By analogy with InlA and InlB, the LRR domain would then be likely to interact with host proteins. The putative binding surface of the LRR domain of InlC is flat and predominantly hydrophilic; associations solely involving hydrophilic and charged residues have been less commonly seen at protein–protein interfaces and if involved in binding, this surface would be involved in relatively weak or transient associations with other molecules (Bahadur *et al.*, 2004). The relatively flat surface of the β-sheet also suggests weak interactions. An involvement in transient interactions or interactions within the cytoplasm might explain why binding partners have yet to be discovered for InlC. Alternatively, the freely accessible Ig-like domain of InlC, unlike the Ig-like domains of InlA and B which are within larger multi-domain proteins, might itself constitute a potential receptor-binding site affording a new method of interaction between the small internalins and their host receptors.

We are grateful to Fredi Engelbrecht and Werner Goebel (Universität Würzburg, Germany) for providing the original

pQE-30::*inlC* construct. We acknowledge the use of the Synchrotron Radiation Source, Daresbury and the ESRF Grenoble. The Higher Education Funding Council for England and the Biotechnology and Biological Sciences Research Council supported this work.

References

Bahadur, R. P., Chakrabarti, P., Rodier, F. & Janin, J. (2004). *J. Mol. Biol.* **336**, 943–955.
Bergmann, B., Raffelsbauer, D., Kuhn, M., Goetz, M., Horn, S. & Goebel, W. (2002). *Mol. Microbiol.* **43**, 557–570.
Braun, L. & Cossart, P. (2000). *Microbes Infect.* **2**, 803–811.
Braun, L., Ohayon, H. & Cossart, P. (1998). *Mol. Microbiol.* **27**, 1077–1087.
Collaborative Computational Project, Number 4 (1994). *Acta Cryst.* D**50**, 760–763.
DeLano, W. L. (2002). *The PyMOL Molecular Visualization System.* DeLano Scientific, San Carlos, CA, USA. http://www.pymol.org.
Esnouf, R. M. (1997). *J. Mol. Graph.* **15**, 132–134.
Evdokimov, A. G., Anderson, D. E., Routzhan, K. M. & Waugh, D. S. (2001). *J. Mol. Biol.* **312**, 807–821.
Engelbrecht, F., Chun, S.-K., Ochs, C., Hess, J., Lottspeich, F., Goebel, W. & Sokolovic, Z. (1996). *Mol. Microbiol.* **21**, 823–837.
Engelbrecht, F., Dickneite, C., Lampidis, R., Gotz, M., DasGupta, U. & Goebel, W. (1998). *Mol. Gen. Genet.* **257**, 186–197.
Holm, L. & Sander, C. (1993). *J. Mol. Biol.* **233**,123–138.
Ireton, K., Payrastre, B., Chap, H., Ogawa, W., Sakaue, H., Kasuga, M. & Cossart, P. (1996). *Science*, **274**, 780–782.
Jones, T. A., Zou, J.-Y, Cowan, S. W. & Kjeldgaard, M. (1991). *Acta Cryst.* A**47**, 110–119.
Kobe, B. & Deisenhofer, J. (1995). *Curr. Opin. Struct. Biol.* **5**, 409–416.
Kraulis, P. J. (1991). *J. Appl. Cryst.* **24**, 946–950.
Laskowski, R. A., MacAuthur, M. W., Moss, D. S. & Thornton, J. M. (1993). *J. Appl. Cryst.* **26**, 283–291.
Leimeister-Wachter, M., Haffner, C., Domann, E., Goebel, W. & Chakraborty, T. (1990). *Proc. Natl Acad. Sci. USA*, **87**, 8336–8340.
Luo, Q., Rauch, M., Marr, A. K., Muller-Altrock, S. & Goebel, W. (2004). *Mol. Microbiol.* **52**, 39–52.
Marino, M., Banerjee, M., Jonquieres, R., Cossart, P. & Ghosh, P. (2002). *EMBO J.* **21**, 5623–5634.
Marino, M., Braun, L., Cossart, P. & Ghosh, P. (1999) *Mol. Cell*, **4**, 1063–1072.
Machner, M. P., Frese, S., Schubert, W.-D., Orian-Rousseau, V., Gherardi, E., Wehland, J., Niemann, H. H. & Heinz, D. W. (2003). *Mol. Microbiol.* **48**, 1525–1536.
Mengaud, J., Dramsi, S., Gouin, E., Vazquez-Boland, J. A., Milon, G. & Cossart, P. (1991). *Mol. Microbiol.* **5**, 2273–2293.
Mengaud, J., Ohayon, H., Gounon, P., Mege, R. M. & Cossart, P. (1996). *Cell*, **84**, 923–932.
Murshudov, G. N., Vagin, A. A. & Dodson, E. J. (1997). *Acta Cryst.* D**53**, 240–255.
Otwinowski, Z. & Minor, W. (1997). *Methods Enzymol.* **276**, 307–326.
Parida, S. K., Domann, E., Rohde, M., Muller, S., Darji, A., Hain, T., Wehland, J. & Chakraborty, T. (1998). *Mol. Microbiol.* **28**, 81–93.
Schubert, W., Göbel, G., Diepholz, M., Darji, A., Kloer, D., Hain, T., Chakraborty, T., Wehland, J., Domann, E. & Heinz, D. W. (2001). *J. Mol. Biol.* **312**, 783–794.
Schubert, W.-D., Urbanke, C., Ziehm, T., Beier, V., Machner, M. P., Domann, E., Wehland, J., Chakraborty, T. & Heinz, D. W. (2002). *Cell*, **111**, 825–836.
Shen, Y., Naujokas, M., Park, M. & Ireton, K. (2000). *Cell*, **103**, 501–510.
Vagin, A. & Teplyakov, A. (1997). *J. Appl. Cryst.* **30**, 1022–1025.